J Geophys (1985) 57:106–117

Journal of Geophysics

The normal modes of a layered, incompressible Maxwell half-space

Detlef Wolf
Department of Physics, University of Toronto, Toronto, Ontario, Canada, M5S 1A7

Abstract. The theory describing the relaxation of an incompressible, layered Maxwell half-space is developed. The approach is based on the analytic solution of the associated elastic model and the subsequent application of the correspondence principle. The viscoelastic theory follows normal-mode theory, which allows the independent and exact determination of the relaxation-time and amplitude spectra for each mode of relaxation. The solution is tested by calculating the response of several models in the wavenumber and spatial domains. The examples are selected with regard to post-glacial adjustment in Fennoscandia and analyse effects caused by (a) varying lithospheric thickness, (b) adding an asthenosphere, (c) increasing lower-mantle viscosity, (d) permitting relaxation of the lower lithosphere or (e) introducing density contrasts at 400-km and 670-km depths.

Key words: Isostasy – Maxwell continuum – Normal modes

Introduction

The rheology of the solid Earth exhibits various forms of departure from perfect elasticity. Whereas, on a time-scale characteristic of seismic-wave propagation, anelastic effects are significant, on a much longer time-scale, the Earth's mantle is widely believed to support flow (creep). Recent experimental evidence of the steady-state creep properties of likely mantle materials suggest that the creep-rate limiting process is rate-dependent and the creep law therefore non-linear (e.g. Weertman and Weertman, 1975; Tullis, 1979). The inference of the creep properties of the Earth's mantle from such experiments is, however, beset with difficulties. One problem is that the chemical and mineralogical constitution of the mantle is poorly known. A severe limitation is also that laboratory creep experiments are necessarily carried out at creep rates which are orders of magnitude higher than the actual rates in the mantle. Large extrapolations from the experimental conditions are therefore necessary. In view of the uncertainties involved in this kind of reasoning it is therefore not clear whether a linear creep mechanism might not apply at the much lower creep rates characteristic of the Earth's mantle.

In the following we will pursue a pragmatic approach and will assume that the Earth's inelastic response is linear. More specifically, we will be concerned with the rheological model that is usually referred to as Maxwell continuum. This type of rheology has proved successful in interpreting the glacio-isostatic relaxation of the Earth's mantle (e.g. Cathles, 1975; Peltier and Andrews, 1976; Nakiboglu and Lambeck, 1982; Wu and Peltier, 1983) and the adjustments of the Earth's thermal lithosphere on a very long time-scale (e.g. Beaumont, 1978; Lambeck and Nakiboglu, 1980; Courtney, 1982). Clearly, our approach cannot prove that the material constituting the Earth's lithosphere or mantle does in fact respond linearly.

The theory describing the load-induced relaxation of a self-gravitating, compressible and pre-stressed Maxwell sphere has recently been summarized (Peltier, 1982). The gravitationally self-consistent model is recommended when analysing deformations associated with the Laurentide glaciation. In the investigation reported here we are, however, concerned with deformations of the Earth not exceeding the scale of the glacially induced depression in Fennoscandia. On this reduced scale, sphericity and self-gravitation are of subordinate importance (Wolf, 1984) and can therefore be neglected. Effects due to compressibility are analysed in Wolf (1985c). The results show that compressibility is significant only during the initial phases of relaxation. This special feature will therefore also be neglected. The significance of the pre-stress term in the equilibrium equations has been studied before (Wolf, 1985a, b) and needs no further discussion.

With these simplifications, the Earth model is reduced to an incompressible, pre-stressed Maxwell half-space. Special solutions for uniform or two-layer Maxwell models (e.g. Nakiboglu and Lambeck, 1982; Wolf, 1984, 1985b) are of some theoretical interest. For data interpretation the availability of a more versatile model is, however, of definite advantage. In the following we will therefore be concerned with the multi-layer Maxwell half-space model. The associated elastic model has recently been re-analysed by Ward (1984). His solution for the deformation also includes the modifications caused by an external gravity field. Previously, such effects, which, for incompressibility, virtually reduce to pre-stress advection, had usually been neglected in elastic half-space approximations (e.g. Kuo, 1969).

In the following section we will develop the theory governing the deformation of an incompressible, pre-stressed, layered elastic half-space. The solution for the associated Maxwell continuum is obtained by using the correspondence principle. The viscoelastic theory closely follows the normal-mode formulation developed by Peltier (1985). This method allows the independent and exact determination of the relaxation times and amplitudes of all normal modes characteristic of any specific model considered. The method is therefore distinctly superior to the approximate collocation method developed in Peltier (1976) and employed by Courtney (1982) in his study of the evolution of sedimentary basins.

After that, several numerical examples will be discussed. They are intended to illustrate the principal effects caused by (a) variations in lithospheric thickness, (b) the insertion of a low-viscosity channel (asthenosphere), (c) changes in lower-mantle viscosity, (d) the relaxation of the lower portion of the thermal lithosphere or (e) the presence of density discontinuities in the upper mantle. The relaxation of the individual models will be illustrated in various diagrams which show amplitude and relaxation-time spectra (wavenumber domain) or vertical surface deflections (spatial domain). This presentation constitutes a systematic and complete compilation of the response characteristics of the main Earth models under discussion, which has not been available before. The numerical values of the model parameters chosen are of relevance to the interpretation of glacio-isostatic adjustment in Fenno-scandia.

Theory

We wish to derive the solution describing the deformation of a pre-stressed, multi-layer elastic half-space subject to an axisymmetric load. The differential equations governing this problem may be written in matrix form. Assuming incompressibility, we obtain the first-order system (Wolf, 1985c)

$$\begin{bmatrix} D & -k & -\frac{1}{\mu} & 0 \\ k & D & 0 & 0 \\ -4\mu k^2 & 0 & D & -k \\ 0 & 0 & k & D \end{bmatrix} \begin{bmatrix} \hat{u}_1 \\ \hat{w}_0 \\ \hat{\sigma}_{rz1} \\ \hat{\sigma}_{zz0} \end{bmatrix} = 0, \tag{1}$$

where $D = d/dz$. Symbols u, w, σ_{rz} and σ_{zz} denote the radial and vertical displacement components and the appropriate components of the *total* perturbation stress $\sigma_{ij} = \sigma_{ij}^{(e)} + \rho g w \delta_{ij}$, where $\sigma_{ij}^{(e)}$ is the usual *elastic* perturbation stress (Wolf, 1985a). Parameter μ is Lamé's second constant (shear modulus) and ρ denotes the density of the continuum. The external gravity field g is assumed to be directed in the positive z-direction. A circumflex denotes Hankel transformation of zeroth or first order, as indicated by the subscript, with k being the Hankel-transform variable or wavenumber. Equation (1) is formally equivalent to the first-order system appropriate to a non-gravitating elastic continuum, for which the general solution is well-known (e.g. Farrell, 1972; Lanczano, 1982, pp. 120–125). In terms of four

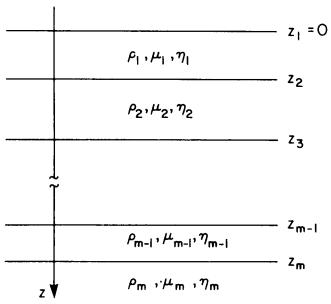

Fig. 1. Multi-layer Maxwell half-space

arbitrary constants, the solution is

$$\begin{bmatrix} \hat{u}_1 \\ \hat{w}_0 \\ \hat{\sigma}_{rz1} \\ \hat{\sigma}_{zz0} \end{bmatrix} = \begin{bmatrix} \pm 1 \\ 1 \\ -2\mu k \\ \pm 2\mu k \end{bmatrix} A_{1,2} \exp(\pm kz), \tag{2a}$$

$$\begin{bmatrix} \hat{u}_1 \\ \hat{w}_0 \\ \hat{\sigma}_{rz1} \\ \hat{\sigma}_{zz0} \end{bmatrix} = \begin{bmatrix} kz \pm 1 \\ \mp kz \\ \pm 2\mu k^2 z + 2\mu k \\ -2\mu k^2 z \end{bmatrix} B_{1,2} \exp(\pm kz). \tag{2b}$$

We first consider a homogeneous elastic half-space extending between $z_m < z < \infty$ (Fig. 1). Then A_1 and B_1 in Eq. (2) vanish. At $z = z_m$ the solution takes the form

$$\mathbf{Y}(z_m) = \mathbf{L}^{(m)} \mathbf{A}, \tag{3}$$

where column matrices

$$\mathbf{Y}(z) = [\hat{u}_1(z), \hat{w}_0(z), \hat{\sigma}_{rz1}(z), \hat{\sigma}_{zz0}(z)]^T, \tag{4}$$

$$\mathbf{A} = [C_1, C_2, 0, 0]^T \tag{5}$$

have been introduced. The symbols C_1 and C_2 designate new constants. Explicit expressions for the elements of the half-space propagator $\mathbf{L}^{(m)}$ are given in Appendix A, Eq. (26). In a similar fashion, the elements at the top $z = z_l$ of the l-th layer (Fig. 1) can be expressed in terms of the quantities at the base $z = z_{l+1}$. Then the general solution, Eq. (2), reduces to

$$\mathbf{Y}(z_l) = \mathbf{L}^{(l)} \mathbf{Y}(z_{l+1}). \tag{6}$$

The elements of the layer propagator $\mathbf{L}^{(l)}$ are given in Appendix A, Eq. (27).

Since *elastic* stress components are continuous across interfaces, it is convenient to modify the equations slightly. If we observe that the elastic stress $\sigma_{ij}^{(e)}$ is connected with the total stress σ_{ij} by $\sigma_{ij} = \sigma_{ij}^{(e)} + \rho g w \delta_{ij}$ (Wolf, 1985a), Eqs. (3) and (6) can be re-written in terms of the elastic stress components. With

$$\mathbf{Y}^{(e)}(z) = [\hat{u}_1(z), \hat{w}_0(z), \hat{\sigma}_{rz1}(z), \hat{\sigma}_{zz0}^{(e)}(z)]^T, \tag{7}$$

we obtain

$$\mathbf{Y}^{(e)}(z_m) = \mathbf{P}^{(m)} \mathbf{A} \tag{8}$$

for the half-space and

$$\mathbf{Y}^{(e)}(z_l) = \mathbf{P}^{(l)} \mathbf{Y}^{(e)}(z_{l+1}) \tag{9}$$

for the l-th layer. The relation between $\mathbf{L}^{(m)}$ and $\mathbf{P}^{(m)}$ is given in Eq. (28), that between $\mathbf{L}^{(l)}$ and $\mathbf{P}^{(l)}$ in Eq. (29), of Appendix A, respectively.

With the requirement that displacement components and elastic stress components be continuous across any interface, the solution for an arbitrary m-layer elastic continuum is now readily constructed from Eqs. (8) and (9). If we number the layers from the top to the base and observe that the m-th basal layer extends towards $z \to \infty$ (Fig. 1), the field quantities at the upper surface $z = z_l$ of the l-th layer may be represented as

$$\mathbf{Y}^{(e)}(z_l) = \mathbf{P}(z_l)\,\mathbf{A}, \tag{10}$$

where

$$\mathbf{P}(z_l) = \sum_{L=l}^{m} \mathbf{P}^{(L)}. \tag{11}$$

Equation (10) can be expressed as a combination of two linearly independent solutions. Remembering the definition of the column matrix $\mathbf{A}$, Eq. (5), and introducing

$$\mathbf{P}_1(z) = [P_{11}(z), P_{21}(z), P_{31}(z), P_{41}(z)]^T, \tag{12a}$$

$$\mathbf{P}_2(z) = [P_{12}(z), P_{22}(z), P_{32}(z), P_{42}(z)]^T, \tag{12b}$$

Eq. (10) becomes

$$\mathbf{Y}^{(e)}(z_l) = C_1\,\mathbf{P}_1(z_l) + C_2\,\mathbf{P}_2(z_l). \tag{13}$$

This constitutes the general solution for the field quantities at the top of the l-th layer.

The arbitrary constants C_1 and C_2 can be determined from the boundary conditions. As usual in geophysical applications, the stress components $\hat{\sigma}_{rz1}$ and $\hat{\sigma}_{zz0}$ are assumed to be known at the top $z = z_1 = 0$ of the upper layer. If the sub-matrix

$$\mathbf{M} = \begin{bmatrix} P_{31}(0) & P_{32}(0) \\ P_{41}(0) & P_{42}(0) \end{bmatrix} \tag{14}$$

is introduced and the definitions

$$\mathbf{B} = [\hat{\sigma}_{rz1}(0), \hat{\sigma}_{zz0}(0)]^T, \tag{15}$$

$$\mathbf{C} = [C_1, C_2]^T \tag{16}$$

are observed, the boundary conditions $\mathbf{B}$ take the form

$$\mathbf{B} = \mathbf{M}\mathbf{C} \tag{17a}$$

or, after inversion,

$$\mathbf{C} = \mathbf{M}^{-1}\,\mathbf{B}. \tag{17b}$$

The inverse matrix $\mathbf{M}^{-1}$ is given by

$$\mathbf{M}^{-1} = (\det \mathbf{M})^{-1}\,\mathbf{M}^A, \tag{18}$$

where $\mathbf{M}^A$ is the adjugate matrix associated with $\mathbf{M}$. Equation (13) and the boundary conditions given by Eq. (17) completely determine the solution.

According to the correspondence principle (e.g. Cathles, 1975, pp. 25–29), Eqs. (13) and (17) can be interpreted as the Laplace-transformed quasi-static solution appropriate to the associated Maxwell continuum subject to impulsive boundary conditions $\mathbf{B}\delta(t)$. In the time domain, the solution takes the form

$$\mathbf{Y}^{(ve)}(t, z_l) = \mathbf{Y}^{(e)}(z_l)\,\delta(t) + \sum_k \mathbf{Y}^{(v,k)}(z_l)\,s^{(k)} \exp(-s^{(k)} t). \tag{19}$$

The eigenvalues $s^{(k)}$ and associated eigenfunctions (normal modes) $\mathbf{Y}^{(v,k)}$ are complicated functions of the model parameters and boundary conditions. For simple Maxwell models they can be explicitly calculated (e.g. Wolf, 1984). For the multi-layer half-space considered here a more general approach is recommended. We employ the normal-mode method developed by Peltier (1985). The details of the calculations are outlined in Appendix B.

In the following we will be concerned with the vertical deflection $\hat{w}_0(t, z_l)$ subject to the boundary condition $\mathbf{B} = [0, -\hat{q}_0]^T$. Since the solution is linear in the load pressure $\hat{q}_0$ (Appendix B), we write

$$\hat{w}_0(t, z_l) = T^{(ve)}(t, z_l)\,\hat{q}_0, \tag{20}$$

where

$$T^{(ve)}(t, z_l) = T^{(e)}(z_l)\,\delta(t) + \sum_k T^{(v,k)}(z_l)\,s^{(k)} \exp(-s^{(k)} t) \tag{21}$$

is the viscoelastic transfer function for impulsive forcing. For a Heaviside unloading event $\hat{q}_0(k)[1 - H(t)]$ we obtain, upon convolution,

$$T^{(ve)}(t, z_l) = \begin{cases} T^{(e)} + \sum_k T^{(v,k)}, & t < 0 \\ \sum_k T^{(v,k)} \exp(-s^{(k)} t), & t > 0 \end{cases}. \tag{22}$$

The Hankel transform of the gravity anomaly Δg at $z = 0$ associated with the deformation of a stack of m layers at $z > 0$ can be approximated by (e.g. Parker, 1972)

$$\Delta \hat{g}_0(t, 0) = G^{(ve)}(t)\,\hat{q}_0, \tag{23}$$

where

$$G^{(ve)}(t) = -2\pi\gamma \sum_{L=1}^{m} [(\rho_L - \rho_{L-1}) \exp(-k z_L) T^{(ve)}(t, z_L)] \tag{24}$$

and γ is the gravitational constant. For $L = 1$, ρ_{L-1} denotes the density of the material (usually air or water) superimposed on the layered half-space.

Numerical examples and discussion

The relaxation of the Earth's surface in response to loads comparable in scale to the Fennoscandian ice-sheet has been widely assumed to be dominated by the viscosity of the upper mantle (e.g. Cathles, 1975, pp. 173–196). The response may, however, be modified by (a) the lithosphere, (b) the presence of a low-viscosity asthenosphere, (c) the viscosity stratification of the low-

Table 1. Parameters of Earth models employed

Layer	h (km)	ρ (kg m^{-3})	μ (N m^{-2})	η (Pa s)
Earth Model A.1				
1	100.0	3,380	0.67×10^{11}	∞
2	100.0	3,380	1.45×10^{11}	η_2
3	∞	3,380	1.45×10^{11}	1.0×10^{21}
Earth Model L.1				
1	h_1	3,380	0.67×10^{11}	∞
2	∞	3,380	1.45×10^{11}	1.0×10^{21}
Earth Model L.2				
1	75.1	3,380	0.67×10^{11}	∞
2	8.7	3,380	0.67×10^{11}	1.0×10^{25}
3	10.3	3,380	0.67×10^{11}	1.0×10^{23}
4	∞	3,380	1.45×10^{11}	1.0×10^{21}
Earth Model L.3				
1	51.8	3,380	0.67×10^{11}	∞
2	14.1	3,380	0.67×10^{11}	1.0×10^{25}
3	20.3	3,380	0.67×10^{11}	1.0×10^{23}
4	∞	3,380	1.45×10^{11}	1.0×10^{21}
Earth Model M.1				
1	100.0	3,380	0.67×10^{11}	∞
2	570.0	3,380	1.45×10^{11}	1.0×10^{21}
3	∞	3,380	1.45×10^{11}	η_3
Earth Model M.2				
1	100.0	3,380	0.67×10^{11}	∞
2	570.0	3,380	1.45×10^{11}	1.0×10^{21}
3	∞	3,770	1.45×10^{11}	1.0×10^{21}
Earth Model M.3				
1	100.0	3,380	0.67×10^{11}	∞
2	300.0	3,380	1.45×10^{11}	1.0×10^{21}
3	270.0	3,560	1.45×10^{11}	1.0×10^{21}
4	∞	3,950	1.45×10^{11}	1.0×10^{21}
Earth Model S				
1	100.0	3,380	0.67×10^{11}	∞
2	∞	3,380	1.45×10^{11}	1.0×10^{21}

er mantle, (d) relaxation near the base of the lithosphere or (e) density discontinuities in the upper mantle.

In this section we will be discussing the characteristic signatures produced by each of these special features successively. In order to have some reference, we proceed from a "standard" model, which is called Earth Model S. It is composed of a 100-km-thick elastic lithosphere overlying a uniformly viscous mantle with a dynamic viscosity of $\eta=10^{21}$ Pa s. The model parameters are listed in Table 1.

Figure 2a shows the viscous transfer functions $T^{(v,k)}(0)$ associated with the two modes of Earth Model S as functions of angular order n. The latter quantity is formally defined by $n=ka$, with a the Earth's radius. The bimodal character of the viscous response of this model was discussed previously. It is characterized by a major mantle branch M0, for which the shear energy has a maximum in the interior of the mantle, and a subordinate lithospheric branch L0, for which the shear energy is concentrated immediately below the base of the lithosphere (Wu and Peltier, 1982; Wolf, 1984). One of the effects of the lithosphere

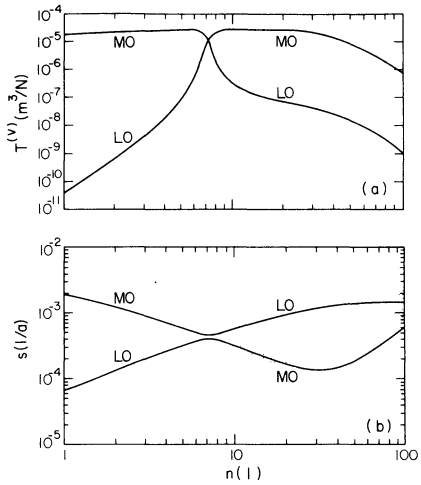

Fig. 2a, b. **a** Viscous transfer function $T^{(v,k)}$ and **b** inverse relaxation time $s^{(k)}$ as function of angular order n for Earth Model S; symbols denote relaxation mode

is that it accelerates the decay of short-wavelength deformations. This is evident from Fig. 2b, which shows that the relaxation time $1/s^{(k)}$ of the M0 mode is substantially shortened at $n>30$.

Most interestingly, such a behaviour is displayed by a relaxation-time estimate based on a spectral decomposition of Pleistocene strandline data from Fennoscandia (McConnell, 1968). Walcott (1980) has, however, pointed out that the short-wavelength part of McConnell's spectrum could also reflect the effects of structural hinge zones on the tilt of the Pleistocene strandlines. Some caution as to the significance of McConnell's estimate is therefore indicated.

In Fig. 2b and the following relaxation-time diagrams the estimate for Fennoscandia is represented as a stippled band. McConnell (1968) based his decomposition on the assumption that the Fennoscandian uplift is governed by a single mode of relaxation. Although this is not strictly correct, his estimate can be compared with the theoretical relaxation-time spectrum of the fundamental mode M0, provided that the later dominates the theoretical response on the time-scale considered. This assumption holds for Earth Model S.

We first investigate the modifications introduced by varying lithospheric thickness (Table 1, Earth Model L.1). In Fig. 3a and b the thickness has been increased to 150 km, whereas in Fig. 3c and d the thickness is 200 km. Since the relative strength of the L0 mode remains insignificant, the relaxation is, as in Earth Model S, governed by the M0 mode. At higher wavenumbers the increase in lithospheric thickness causes a decrease in strength of the M0 mode and a shortening of its relaxation time. McConnell's (1968) relaxation-time estimate is best satisfied by a lithosphere of 100-km thickness. This implies that the wavenumber at which relaxation time reaches a maximum is used as the primary criterion for the goodness of the fit.

Figure 4 illustrates the modifications of the basic response of Earth Model S produced by inserting a 100-km-thick asthenosphere below the lithosphere (Table 1, Earth Model A.1). In Fig. 4a and b the asthenosphere has a viscosity of 5×10^{19} Pa s; in Fig. 4c and d

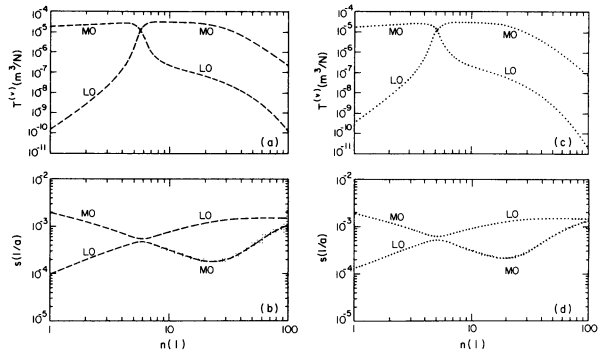

Fig. 3a–d. Same as Fig. 2 except for Earth Model L.1 with $h_1 = 150$ km (*dashed*) or $h_1 = 200$ km (*dotted*)

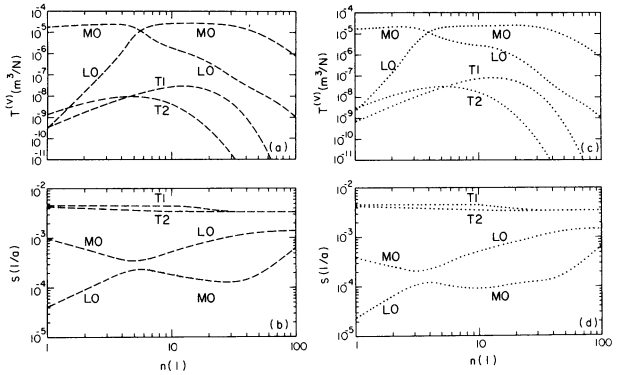

Fig. 5a–d. Same as Fig. 2 except for Earth Model M.1 with $\eta_3 = 2 \times 10^{21}$ Pa s (*dashed*) or $\eta_3 = 5 \times 10^{21}$ Pa s (*dotted*)

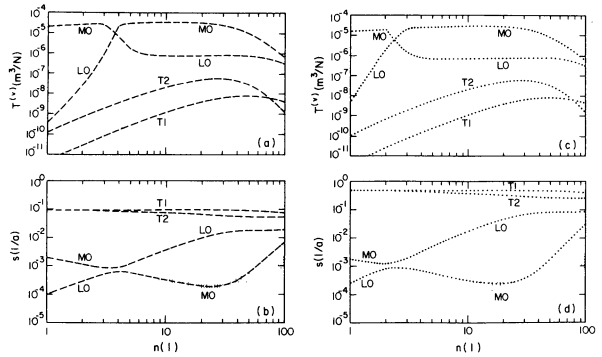

Fig. 4a–d. Same as Fig. 2 except for Earth Model A.1 with $\eta_2 = 5 \times 10^{19}$ Pa s (*dashed*) or $\eta_2 = 1 \times 10^{19}$ Pa s (*dotted*)

the viscosity is 1×10^{19} Pa s. The presence of an asthenosphere adds two modes of short relaxation time. Following Peltier (1976), we call such modes transition modes ("T modes"). Figure 4a and c shows that they are only poorly excited. The main modification introduced by the asthenosphere is therefore a shortening of the relaxation time of the fundamental mode M0 at $n > 30$ (see also McConnell, 1968). A comparison between Figs. 3 and 4 further suggests that there may exist a certain trade-off between lithospheric thickness and asthenospheric thickness so that the response is nearly unchanged, provided that the total thickness of lithosphere and asthenosphere remains approximately constant. To what extent this statement is correct will be discussed later, when the deformation in the spatial domain is discussed.

For completeness, the effects caused by increasing the viscosity of the lower mantle are also considered (Table 1, Earth Model M.1), although this model is physically equivalent to Earth Model A.1. In Fig. 5a and b the viscosity below a depth of 670 km is 2×10^{21} Pa s; in Fig. 5c and d it is 5×10^{21} Pa s. The main modification, compared with Earth Model S, are the longer relaxation times of the M0 mode at small wavenumbers (Fig. 5b and d). This effect is well-known (e.g. McConnell, 1965). The transition modes, which are not observed for Newtonian viscous continua, are again barely excited and can be neglected when calculating the response in the spatial domain.

The model of a perfectly elastic or *mechanical* lithosphere employed so far is an idealization whose justification is governed by the time-scale of the external forcing. Whereas the model is clearly inadequate to sedimentary loads, it has generally been used when modeling glacio-isostatic adjustment.

In order to analyse the influence of relaxation near the base of the lithosphere, we develop a more realistic model. It is based on the fact that creep is a temperature-activated process. Then, from Appendix C, Eq. (47b), we have for the viscosity η of the material considered

$$\eta(T) = \eta_0 \exp[Q(1/T - 1/T_0)/R], \tag{25}$$

where $\eta_0 = \eta(T_0)$. In the present context Q denotes the activation energy of the lithospheric material, T is the absolute temperature in the lithosphere and R the gas constant. If a characteristic geotherm $T = T(z)$ is substituted, $\eta = \eta(z)$ is obtained. This method of estimating the viscosity-depth distribution in the lithosphere was previously employed by Courtney (1982), who studied the response of the thermal lithosphere in connection with the evolution of sedimentary basins.

Geologically, a large portion of Fennoscandia is a Precambrian shield. Therefore, the "old" continental geotherms discussed by Sclater et al. (1980) may serve as a guide-line when modeling subsurface temperatures in this region. For our purposes their geotherms may be approximated by a linear function which passes through the points $T = 0°$ C, $z = 0$ km and $T = 1{,}000°$ C, $z = 100$ km.

Recent laboratory estimates of the activation energy for materials believed to be typical of the Earth's crust or mantle have, for example, been compiled by Tullis (1979). Most of the samples have activation energies which range between 200 and 500 kJ mol^{-1}. The lower values are usually associated with more silicic minerals, whereas the higher values are appropriate to olivine.

Figure 6 shows viscosity-depth distributions for different values of Q. If we define the *thermal* lithosphere as that part of the Earth's outer shell where $\eta > 10^{21}$ Pa s, its thickness is 100 km in the models considered. The underlying mantle has a uniform viscosity of 10^{21} Pa s. If $Q \to \infty$ in the lithosphere, $\eta \to \infty$ and Earth Model S is recovered. For $Q = 500$ kJ mol^{-1}, the viscosity-depth distribution is less abrupt; if $Q = 200$

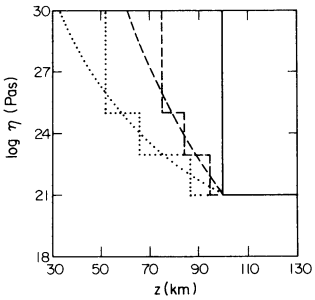

Fig. 6. Viscosity η as function of depth z for $Q \to \infty$ (*solid*), $Q = 500$ kJ mol^{-1} (*dashed*) or $Q = 200$ kJ mol^{-1} (*dotted*); exponential distributions are approximated by three uniform layers

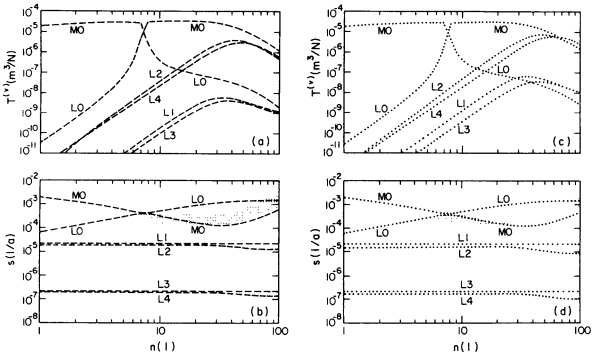

Fig. 7a–d. Same as Fig. 2 except for Earth Model L.2 (*dashed*) or Earth Model L.3 (*dotted*)

kJ mol^{-1}, the thickness of the region of intermediate viscosity near the base of the thermal lithosphere is further increased. Clearly, the value of Q is quite significant. Since silicic material is believed to be concentrated in the upper crust, $Q = 500$ kJ mol^{-1} might be more realistic for the lower lithosphere. For computational ease, the exponential distributions are approximated by three layers of constant viscosity (Fig. 6; Table 1, Earth Models L.2 and L.3). In the upper layer we have, as before, $\eta \to \infty$; in the middle layer $\eta = 10^{25}$ Pa s, whereas in the lower layer $\eta = 10^{23}$ Pa s.

The response of the two models is displayed in Fig. 7a and b (Earth Model L.2) and in Fig. 7c and d (Earth Model L.3). A comparison with Fig. 2 shows that the relaxation-time and amplitude spectra of the M0 and L0 modes remain virtually unchanged. Each layer, however, causes a pair of new modes. Since they are related to the rheological stratification of the lithosphere, they are of the L-type. We have chosen to number them in order of increasing relaxation time. If $n > 40$, the amplitudes of the L2 and L4 modes are comparable to the amplitude of the M0 mode, whereas their relaxation times are much longer. Due to the approximations involved in the previously mentioned collocation method, Courtney (1982) could not determine the strength of the weaker lithospheric modes. As shown here, their contribution is, however, insignificant.

The main modification of the relaxation pattern produced by internal, non-adiabatic density contrasts is that each such contrast is associated with a characteristic relaxation mode (Parsons, 1972; Peltier, 1976; Wu

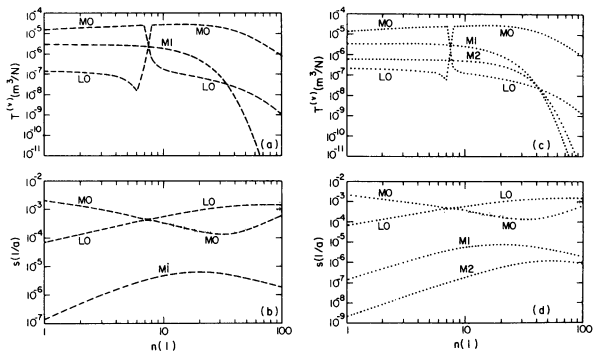

Fig. 8a–d. Same as Fig. 2 except for Earth Model M.2 (*dashed*) or Earth Model M.3 (*dotted*)

and Peltier, 1982). Since the density discontinuities in the upper mantle are about one order of magnitude smaller than the discontinuity at the Earth's surface, the buoyancy effects are also smaller. Thus, the modes associated with non-adiabatic density stratification in the interior are expected to decay much slower than the M0 mode.

In the following, density contrasts of 180 kg m^{-3} and 390 kg m^{-3} will be introduced at 400-km and 670-km depth, respectively (Table 1, Earth Models M.2 and M.3). This choice is consistent with the PREM model of the elastic structure of the Earth (Dziewonski and Anderson, 1981). The superimposed gradual increase in density with depth in the upper mantle is believed to be primarily due to adiabatic compression. It therefore does not interfere with our incompressible analysis.

In Earth Model M.2 only the larger internal density contrast at 670-km depth has been included (Fig. 8a and b). The M1 mode associated with this discontinuity has a relaxation time of the order of 1 Ma. For $n < 10$ it carries about 10% of the strength of the M0 mode. Deformations of shorter wavelength do not sample deeply enough to excite the M1 mode appreciably. In Earth Model M.3 the discontinuity at 400 km has been added (Fig. 8c and d). This causes a second internal mode M2 which, however, decays exceedingly slowly and carries even less energy than the M1 mode.

In the following, a systematic comparison of the response characteristics in the spatial domain of the different Earth models will be presented. Previously, only isolated cases were discussed in the literature. The examples discussed here apply to a square-edged disk load with a radius of $R = 600$ km. This approximates the scale of the Fennoscandian ice-sheet during the period of stagnation between 10 and 12 ka B.P. (e.g. Cathles, 1975, p. 127). The thickness of the disk is $h_0 = 2$ km. This corresponds to the average thickness of an ice-sheet of parabolic cross-section and 3-km axial thickness. The load density is 1,000 kg m^{-3}.

In calculating the deflection curves shown in Figs. 10 and 11, a Heaviside unloading event of the form $1 - H(t)$ has been assumed. The load is therefore assumed to have acted for an infinite period of time before it is instantaneously removed at $t = 0$ (Fig. 9a). This simulates the rapid disintegration of the Fennoscandian ice-sheet following the period of stagnation. The vertical surface deflection is obtained after taking the inverse Hankel transform (e.g. Wolf, 1985c).

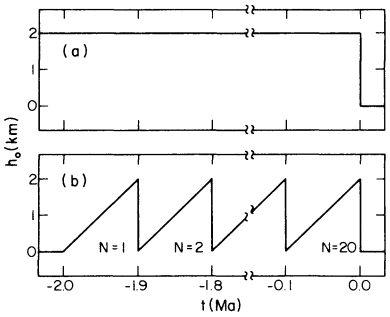

Fig. 9a, b. **a** Heaviside unloading event applicable to Figs. 10 and 11 and **b** saw-tooth loading history applicable to Figs. 12–17

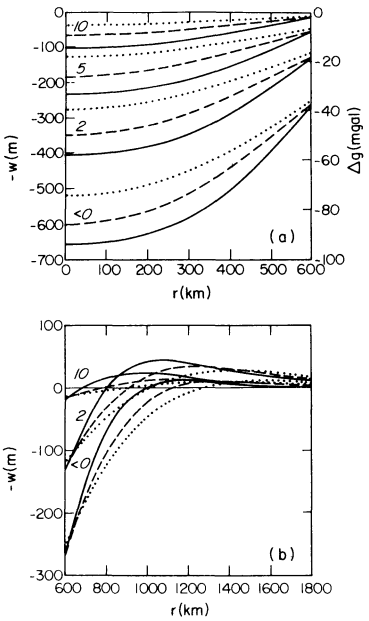

Fig. 10a, b. Vertical surface displacement w as function of distance r from load axis for **a** central or **b** peripheral region and for several times (in units of ka) after load removal; deflection curves refer to Earth Model S (*solid*) or to Earth Model L.1 with $h_1 = 150$ km (*dashed*) or $h_1 = 200$ km (*dotted*); free-air gravity anomaly Δg is indicated for central region; results apply to Heaviside unloading event of Fig. 9a

In Fig. 10 the surface deflection for Earth Model S is compared with that for Earth Model L.1. The influence of lithospheric thickness on the magnitude of the deflection is substantial. This is a simple consequence of the filtering effect of the lithosphere, which, with increasing thickness, becomes less "transparent" for deformations of shorter wavelength (Fig. 3a and c). As the only density jump is at the Earth's surface, the gravity anomaly can be determined directly from $\Delta g(t, 0) = 2\pi\gamma\rho_1 w(t, 0)$. Since $\rho_1 = 3{,}380\ \mathrm{kg\ m^{-3}}$, a downward deflection of 70 m almost exactly corresponds to a free-air gravity anomaly of -10 mgal. The peak anomaly associated with the present ($t = 10$ ka) degree of disequilibrium in Fennoscandia is probably around -15 mgal (Balling, 1980). From Fig. 10a it is thus obvious that, on the basis of the elementary model employed, lithospheric thicknesses in excess of 150 km are difficult to reconcile with the gravity data.

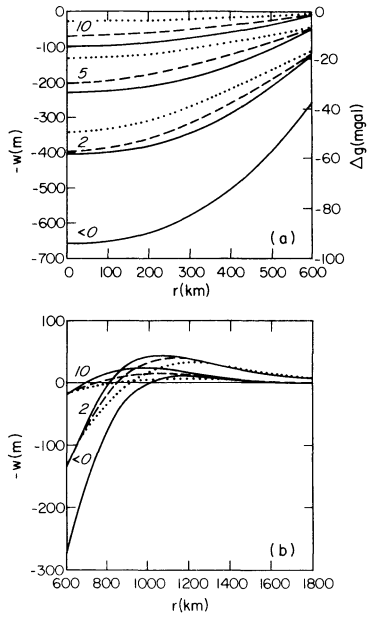

Fig. 11a, b. Same as Fig. 10 except that Earth Model A.1 with $\eta_2 = 5 \times 10^{19}$ Pa s (*dashed*) or $\eta_2 = 1 \times 10^{19}$ Pa s (*dotted*) is compared with Earth Model S (*solid*)

The signature produced by an asthenosphere is illustrated in Fig. 11, which compares Earth Models S and A.1. As mentioned previously, the modification of the relaxation-time spectrum of the M0 mode produced by an asthenosphere is similar to the effect produced by an increase in the thickness of the lithosphere. Due to differences in the amplitude spectra, the response characteristics in the spatial domain are, nevertheless, distinct. As opposed to the modifications caused by increasing lithospheric thickness, there is, in particular, no effect of the asthenosphere on the initial deflection. This is because the equilibrium deflection at $t < 0$ must necessarily be independent of the viscosity stratification of the mantle and is only dependent on the thickness and the elastic structure of the lithosphere.

In the peripheral region the presence of an asthenosphere reduces the inward shift of the zero-crossing associated with the relaxation of Earth Model S considerably (Fig. 11b). The influence of the asthenosphere is, however, not strong enough to counteract the initially sympathetic uplift of this region for Earth Model S effectively (see also Cathles, 1975, pp. 184–191).

For a demonstration of the response characteristics produced by modifications (c), (d) and (e) (see beginning of this section) it is necessary to employ a higher approximation for the loading history. This is because the associated models support slowly decaying modes. Then the relaxation is no longer governed exclusively by the details of the deglaciation event but also markedly influenced by the long-term accumulation and ablation history of the ice-sheet.

Oxygen-isotope data from deep-sea sedimentary cores suggest that the recent ice age started approximately 2 Ma B.P. and consisted of individual glaciations of about 100-ka duration [see Imbrie and Imbrie (1979) for a summary]. A reasonable approximation to the complete sequence is the saw-tooth loading history shown in Fig. 9b. In the glaciation model we have

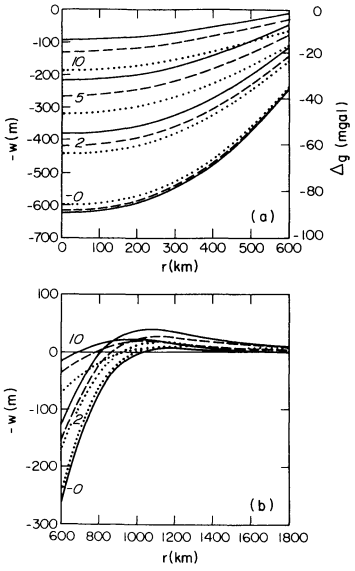

Fig. 12a, b. Vertical surface displacement w as function of distance r from load axis for **a** central or **b** peripheral region and for several times (in units of ka) after load removal; deflection curves refer to Earth Model S (*solid*) or to Earth Model M.1 with $\eta_3 = 2 \times 10^{21}$ Pa s (*dashed*) or $\eta_3 = 5 \times 10^{21}$ Pa s (*dotted*); free-air gravity anomaly Δg is indicated for central region; results apply to saw-tooth loading history of Fig. 9b

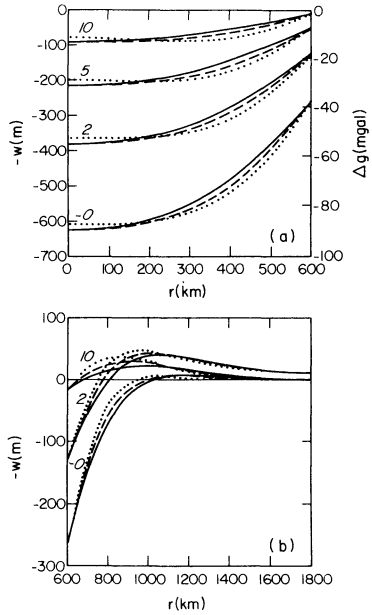

Fig. 13a, b. Same as Fig. 12 except that Earth Model L.2 (*dashed*) or Earth Model L.3 (*dotted*) is compared with Earth Model S (*solid*)

adopted exactly 20 cycles, where each cycle is assumed to have lasted for 100 ka. During each cycle the thickness of the straight-edged disk builds up linearly, whereas its radius is assumed to remain constant. This is a very good approximation to a more complicated model which incorporates effects due to variations of the radius (Wu and Peltier, 1983).

In order to facilitate comparisons with Figs. 10 and 11 the load radius has been kept at 600 km in the calculations underlying the following figures. It must, however, be pointed out that, at least at the time of the last glacial maximum about 18 ka B.P., the Fennoscandian ice-sheet extended south to North Germany. A somewhat larger radius might therefore be more appropriate.

Figure 12 shows the relaxation following the final cycle in the glaciation sequence of Fig. 9b for Earth Model M.1. As expected, the initial displacement is slightly reduced compared with Earth Model S. During relaxation this situation is, however, reversed, and Earth Model M.1 is characterized by considerably enhanced residual deformation. Since the significance of the lower mantle for post-glacial uplift in Fennoscandia has not always been appreciated in the past (e.g. Parsons, 1972), the demonstrated sensitivity of the response to the viscosity structure of the lower mantle should help further clarify this aspect. Figure 12b provides additional information and demonstrates that the inward movement of the zero-crossing of the displacement curve for Earth Model S is suppressed almost completely if the lower-mantle viscosity is increased by a factor of five. This characteristic feature was discussed previously with respect to relative-sea-level data from the North American east coast (Peltier, 1974).

In Fig. 13 the modifications introduced by permitting the relaxation of the lower portions of the thermal lithosphere are shown. As expected, the relaxation after the final loading cycle resembles that associated with a perfectly elastic but thinner lithosphere. In our example the magnitude and tilt of the deflection in the marginal and peripheral regions of the load are very sensitive to the relaxation of the thermal lithosphere. This is consistent with the spectral-response characteristics (Fig. 7), according to which only shorter-wavelength deformations are markedly affected by the L1 and L2 modes. It is, however, important to realize that the details of the modifications of the response in the spatial domain depend strongly on the thickness of the thermal lithosphere and the lateral scale of the load adopted. Suitable combinations of both parameters may, therefore result in effects quite different from those described here.

In order to address the influence of the slowly decaying M1 and M2 modes associated with the 670-km and 400-km density discontinuities, respectively, we again employ the saw-tooth loading history (Fig. 9b). Figure 14a shows that the axial surface displacement associated with Earth Models M.2 and M.3 builds up gradually and, after about 10 cycles, has almost become stationary. The decay of the deflections at 400-km depth (Fig. 14b) and 670-km depth (Fig. 14c) with increasing number of load cycles can be understood from the fact that, physically, the M1 and M2 modes are buoyancy effects caused by disequilibrium at the interfaces. The internal modes will therefore "work" towards restoring equilibrium at the interfaces, which, in our case, corresponds to a plane interface.

The decay of the axial deflection after the final loading cycle is shown in Fig. 15. On the time-scale considered, the modifications introduced by the slowly decaying M1 and M2 modes just start to become visible in the surface deflection at $t = 10$ ka (Fig. 15a). At

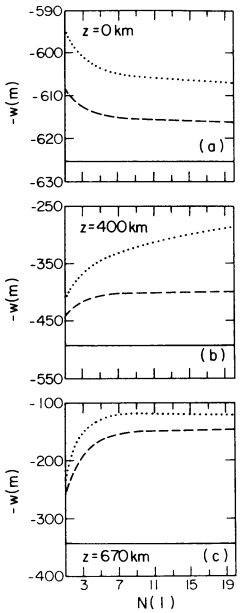

Fig. 14a–c. Axial displacement w as function of cycle number N (Fig. 9b) for Earth Model S (*solid*), Earth Model M.2 (*dashed*) or Earth Model M.3 (*dotted*); deflections refer to end of respective cycle but are represented as continuous lines; results apply to **a** $z=0$ km, **b** $z=400$ km or **c** $z=670$ km

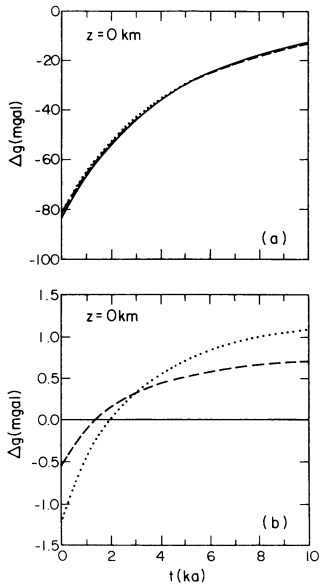

Fig. 16a, b. Axial free-air gravity anomaly Δg as function of time t after load removal (Fig. 9b) for Earth Model S (*solid*), Earth Model M.2 (*dashed*) or Earth Model M.3 (*dotted*); curves show gravity anomaly due to **a** surface density contrast or **b** density contrasts at 400-km and 670-km depths

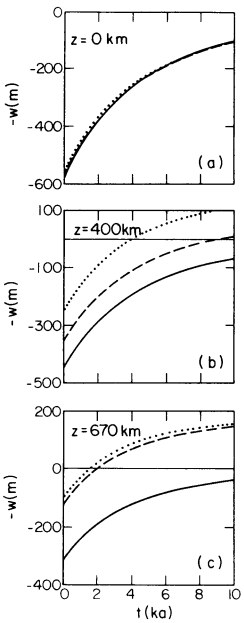

Fig. 15a–c. Axial displacement w as function of time t after load removal (Fig. 9b) for Earth Model S (*solid*), Earth Model M.2 (*dashed*) or Earth Model M.3 (*dotted*); results apply to **a** $z=0$ km, **b** $z=400$ km or **c** $z=670$ km

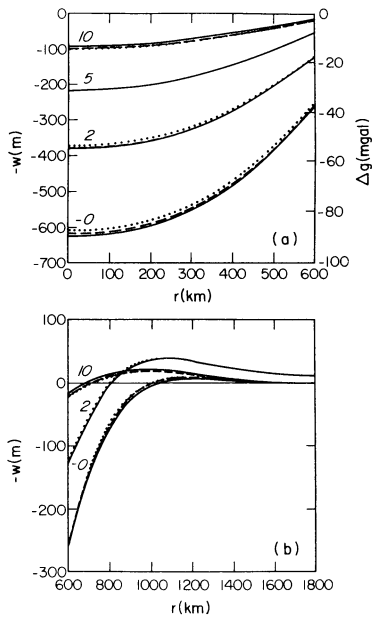

Fig. 17a, b. Same as Fig. 12 except that Earth Model M.2 (*dashed*) or Earth Model M.3 (*dotted*) is compared with Earth Model S (*solid*)

400-km depth (Fig. 15b) and 670-km depth (Fig. 15c) the M0 mode results in upward (positive) vertical displacements after several thousand years. This in turn causes a positive contribution to the gravity anomaly. In the example discussed here its magnitude is, however, very small compared with the negative anomaly related to the first-order density discontinuity at the top surface (Fig. 16) and is therefore neglected in the following figure.

Figure 17 compares the final relaxation of the depression for Earth Models S, M.2 and M.3. The effect of the M1 and M2 modes is very small in our example. At larger times and for loads of larger diameter they will become more important, however. An appropriate example is the Laurentide glaciation, where the contribution of the M1 and M2 modes is essential for the explanation of the substantial free-air gravity anomaly correlated with this Pleistocene ice-sheet (Wu and Peltier, 1983).

Conclusion

Our discussion has demonstrated that, for loads comparable in dimension to the Fennoscandian ice-sheet, the influence of the lithosphere on the predicted surface deflection is pronounced. This is at variance with Cathles' analysis, who concluded "that the magnitude of the lithosphere's flexural rigidity is not sufficient to affect the central uplift of the larger Pleistocene loads (Fennoscandia or larger)" (Cathles, 1975, pp. 153–154). Whereas his statement is correct for the Laurentide glaciation (Wolf, 1984), post-glacial uplift of the central region in Fennoscandia may even be suitable for "measuring" lithospheric thickness.

Due to the reduced scale of the load, the Fennoscandian uplift should also be highly sensitive to the presence of an asthenosphere. As demonstrated, the modifications produced in the uplift pattern are distinct from those caused by increasing lithospheric thickness. The characteristic differences are, however, mainly confined to the initial period of isostatic recovery immediately after load removal. High-quality uplift data from this time interval are therefore required. Unfortunately, the initial period of recovery is also strongly affected by the largely unknown details of the deglaciation event (e.g. Wolf, 1985d).

The sensitivity of the response to the viscosity of the lower mantle is in accordance with results obtained by Nakiboglu and Lambeck (1982). Studying the relaxation of a viscoelastic channel underlain by a rigid half-space, they found that the response approaches the half-space limit if the channel thickness exceeds the load radius by about a factor of three.

The relaxation of the lower portions of the thermal lithosphere may turn out to be of some relevance for the interpretation of post-glacial-adjustment data. This may particularly apply if the thermal lithosphere is thicker than 100 km. As shown in the previous section, the axial deflection is substantially reduced by a thick lithosphere. Then lithospheric relaxation may also be efficient near the load axis. Since the relaxation of the higher L modes is exceedingly slow, relative-uplift observations after deglaciation are necessarily nearly unaffected by these modes. The free-air gravity anomaly, on the other hand, is a measure of the absolute deformation. It is therefore expected to be sensitive to lithospheric relaxation. This may be of some consequence for the interpretation of post-glacial-adjustment data from Fennoscandia, where the relation between relative-uplift and gravity observations has been controversial (e.g. Cathles, 1975, pp. 151–154).

Internal density contrasts have been shown to be of minor importance to the interpretation of post-glacial adjustment, provided that the load radius does not exceed 600 km. This result is expected to be slightly modified if somewhat larger load-scales are considered.

Appendix A

Propagator matrices for multi-layer elastic half-space

The non-zero elements of the half-space propagator $\mathbf{L}^{(m)}$ are

$$L_{11}^{(m)} = -1/(2\mu_m k), \tag{26a}$$

$$L_{12}^{(m)} = 1/(2\mu_m k), \tag{26b}$$

$$L_{21}^{(m)} = -1/(2\mu_m k), \tag{26c}$$

$$L_{31}^{(m)} = 1, \tag{26d}$$

$$L_{32}^{(m)} = -1, \tag{26e}$$

$$L_{41}^{(m)} = 1. \tag{26f}$$

Parameter μ_m denotes the shear modulus appropriate to the half-space.

The elements of the layer propagator $\mathbf{L}^{(l)}$ are

$$L_{11}^{(l)} = -kh_l \sinh(kh_l) + \cosh(kh_l), \tag{27a}$$

$$L_{12}^{(l)} = -kh_l \cosh(kh_l), \tag{27b}$$

$$L_{13}^{(l)} = -1/(2\mu_l k)[kh_l \cosh(kh_l) + \sinh(kh_l)], \tag{27c}$$

$$L_{14}^{(l)} = 1/(2\mu_l k)\, kh_l \sinh(kh_l), \tag{27d}$$

$$L_{21}^{(l)} = kh_l \cosh(kh_l), \tag{27e}$$

$$L_{22}^{(l)} = -kh_l \sinh(kh_l) + \cosh(kh_l), \tag{27f}$$

$$L_{23}^{(l)} = -1/(2\mu_l k)\, kh_l \sinh(kh_l), \tag{27g}$$

$$L_{24}^{(l)} = 1/(2\mu_l k)[kh_l \cosh(kh_l) - \sinh(kh_l)], \tag{27h}$$

$$L_{31}^{(l)} = -2\mu_l k[kh_l \cosh(kh_l) + \sinh(kh_l)], \tag{27i}$$

$$L_{32}^{(l)} = 2\mu_l k^2 h_l \sinh(kh_l), \tag{27j}$$

$$L_{33}^{(l)} = kh_l \sinh(kh_l) + \cosh(kh_l), \tag{27k}$$

$$L_{34}^{(l)} = -kh_l \cosh(kh_l), \tag{27l}$$

$$L_{41}^{(l)} = -2\mu_l k^2 h_l \sinh(kh_l), \tag{27m}$$

$$L_{42}^{(l)} = 2\mu_l k[kh_l \cosh(kh_l) - \sinh(kh_l)], \tag{27n}$$

$$L_{43}^{(l)} = kh_l \cosh(kh_l), \tag{27o}$$

$$L_{44}^{(l)} = -kh_l \sinh(kh_l) + \cosh(kh_l). \tag{27p}$$

Parameter μ_l denotes the shear modulus of the l-th layer and $h_l = z_{l+1} - z_l$ is its thickness.

The elements of $\mathbf{P}^{(m)}$ differing from the corresponding elements of $\mathbf{L}^{(m)}$ are

$$P_{41}^{(m)} = L_{41}^{(m)} - \rho_m g L_{21}^{(m)}, \tag{28a}$$

$$P_{42}^{(m)} = L_{42}^{(m)} - \rho_m g L_{22}^{(m)}, \tag{28b}$$

where ρ_m denotes the density of the homogeneous half-space.

The elements of $\mathbf{P}^{(l)}$ differing from the corresponding elements of $\mathbf{L}^{(l)}$ are

$$P_{12}^{(l)} = L_{12}^{(l)} + \rho_l g L_{14}^{(l)}, \tag{29a}$$

$$P_{22}^{(l)} = L_{22}^{(l)} + \rho_l g L_{24}^{(l)}, \tag{29b}$$

$$P_{32}^{(l)} = L_{32}^{(l)} + \rho_l g L_{34}^{(l)}, \tag{29c}$$

$$P_{41}^{(l)} = L_{41}^{(l)} - \rho_l g L_{21}^{(l)}, \tag{29d}$$

$$P_{42}^{(l)} = L_{42}^{(l)} - \rho_l g (L_{22}^{(l)} - L_{44}^{(l)}) - (\rho_l g)^2 L_{24}^{(l)}, \tag{29e}$$

$$P_{43}^{(l)} = L_{43}^{(l)} - \rho_l g L_{23}^{(l)}, \tag{29f}$$

$$P_{44}^{(l)} = L_{44}^{(l)} - \rho_l g L_{24}^{(l)}, \tag{29g}$$

where ρ_l denotes the density of the l-th layer.

Appendix B

Normal modes of layered Maxwell continuum

Following Peltier (1985) we write for Eqs. (13) and (17b), respectively,

$$\tilde{\mathbf{Y}}^{(ve)}(s, z_l) = C_1(s)\, \mathbf{P}_1(s, z_l) + C_2(s)\, \mathbf{P}_2(s, z_l), \tag{30}$$

$$\mathbf{C}(s) = \mathbf{M}^{-1}(s)\, \mathbf{B}, \tag{31}$$

where the transformation $\mu \to \mu s/(s+\tau^{-1})$ (with $\tau = \eta/\mu$ the Maxwell time and s the Laplace-transform variable), and therefore $\mathbf{P} \to \mathbf{P}(s)$ and $\mathbf{M} \to \mathbf{M}(s)$, has been applied. Vector $\tilde{\mathbf{Y}}^{(ve)}$ is the Laplace transform of the "viscoelastic" column matrix, viz.

$$\tilde{\mathbf{Y}}^{(ve)}(s, z) = [\tilde{\tilde{u}}_1(s, z), \tilde{\tilde{w}}_0(s, z), \tilde{\tilde{\sigma}}_{rz1}(s, z), \tilde{\tilde{\sigma}}^{(ve)}_{zz0}(s, z)]^T. \tag{32}$$

Since

$$C_i(s) = \sum_j [\det \mathbf{M}(s)]^{-1} [\mathbf{M}^A(s)]_{ij} B_j, \tag{33}$$

substitution for C_i in Eq. (30) yields

$$\tilde{\mathbf{Y}}^{(ve)}(s, z_l) = [\det \mathbf{M}(s)]^{-1} \mathbf{Q}(s, z_l), \tag{34}$$

where

$$\mathbf{Q}(s, z_l) = \sum_{ij} [\mathbf{M}^A(s)]_{ij} B_j \mathbf{P}_i(s, z_l). \tag{35}$$

From $\lim_{S \to \infty} \mu(s) = \mu$ it follows that

$$\mathbf{Y}^{(e)}(z_l) = \lim_{S \to \infty} \tilde{\mathbf{Y}}^{(ve)}(s, z_l). \tag{36}$$

With

$$\mathbf{Q}^{(v)}(s, z_l) = \det \mathbf{M}[\mathbf{Y}^{(ve)}(s, z_l) - \mathbf{Y}^{(e)}(z_l)], \tag{37}$$

Eq. (34) may then be written as

$$\tilde{\mathbf{Y}}^{(ve)}(s, z_l) = \mathbf{Y}^{(e)}(z_l) + [\det \mathbf{M}(s)]^{-1} \mathbf{Q}^{(v)}(s, z_l). \tag{38}$$

The time-domain solution associated with Eq. (38) is

$$\mathbf{Y}^{(ve)}(t, z_l) = \mathbf{Y}^{(e)}(z_l)\, \delta(t) + 1/(2\pi i) \int_B [\det \mathbf{M}(s)]^{-1} \cdot \mathbf{Q}^{(v)}(s, z_l) \exp(s t)\, ds, \tag{39}$$

where B denotes the Bromwich path. According to the residue theorem this, however, is equivalent to

$$\mathbf{Y}^{(ve)}(t, z_l) = \mathbf{Y}^{(e)}(z_l)\, \delta(t) + \sum \text{res}\, \{[\det \mathbf{M}(s)]^{-1} \mathbf{Q}^{(v)}(s, z_l) \exp(st)\}. \tag{40}$$

If $\mathbf{Q}^{(v)}(s, z_l) \exp(st)$ is regular and $\det \mathbf{M}(s)$ has simple zeros at $-s^{(k)}$, where $s^{(k)} > 0$, we therefore obtain

$$\mathbf{Y}^{(ve)}(t, z_l) = \mathbf{Y}^{(e)}(z_l)\, \delta(t) + \sum_k \frac{Q^{(v)}(-s^{(k)}, z_l) \exp(-s^{(k)} t)}{\left[\frac{d}{ds} \det \mathbf{M}(s)\right]_{s=-s^{(k)}}}. \tag{41}$$

Defining

$$s^{(k)} \mathbf{Y}^{(v,k)}(z_l) = \left\{\left[\frac{d}{ds} \det \mathbf{M}(s)\right]_{s=-s^{(k)}}\right\}^{-1} \mathbf{Q}^{(v)}(-s^{(k)}, z_l), \tag{42}$$

Eq. (41) may alternatively be written in the form

$$\mathbf{Y}^{(ve)}(t, z_l) = \mathbf{Y}^{(e)}(z_l)\, \delta(t) + \sum_k \mathbf{Y}^{(v,k)}(z_l)\, s^{(k)} \exp(-s^{(k)} t). \tag{43}$$

This is the impulse response of the Maxwell half-space.

Appendix C

Viscosity stratification of lithosphere

The one-dimensional form of the stress-strain relation for linear creep can be written as (e.g. Weertman and Weertman, 1975)

$$\dot{\varepsilon} = AD\sigma/(2\mu), \tag{44}$$

with σ the stress and $\dot{\varepsilon}$ the strain rate. Parameter A is an empirical constant depending weakly on temperature. Parameter D is the diffusion coefficient of the material given by

$$D = D_\infty \exp[-Q/(RT)], \tag{45}$$

with Q the activation energy, R the gas constant and T the absolute temperature. Substituting for D in Eq. (45) yields

$$\dot{\varepsilon} = AD_\infty \sigma \exp[-Q/(RT)]/(2\mu). \tag{46}$$

The effective viscosity is defined by $\eta = \sigma/(2\dot{\varepsilon})$. Substituting for $\sigma/(2\dot{\varepsilon})$ from Eq. (46) we obtain

$$\eta(T) = \eta_\infty \exp[Q/(RT)], \tag{47a}$$

where $\eta_\infty = \mu/(AD_\infty)$. If the viscosity $\eta_0 = \eta(T_0)$ is known, Eq. (47a) may alternatively be written as

$$\eta(T) = \eta_0 \exp[Q(1/T - 1/T_0)/R]. \tag{47b}$$

Acknowledgements. I would like to thank Richard Peltier, who provided a preprint which describes the normal-mode formalism and who called my attention to the possible significance of lithospheric relaxation. This research was financially supported by a Natural Sciences and Engineering Research Council of Canada Postgraduate Scholarship.

References

Balling, N.: The land uplift in Fennoscandia, gravity field anomalies and isostasy. In: Earth rheology, isostasy, and eustasy, N.-A. Mörner, ed.: pp. 297–321. New York: Wiley 1980

Beaumont, C.: The evolution of sedimentary basins on a viscoelastic lithosphere: theory and examples. Geophys. J.R. Astron. Soc. **55**, 471–497, 1978

Cathles, L.M.: The viscosity of the Earth's mantle. Princeton: Princeton University Press 1975

Courtney, R.C.: On the rheology of the oceanic and continental lithospheres. M.Sc. thesis, Dalhousie University 1982

Dziewonski, A.M., Anderson, D.L.: Preliminary reference Earth model. Phys. Earth Planet. Inter. **25**, 297–356, 1981

Farrell, W.E.: Deformation of the Earth by surface loads. Rev. Geophys. Space Phys. **10**, 761–797, 1972

Imbrie, J., Imbrie, K.P.: Ice ages: solving the mystery. Hillside: Enslow 1979

Kuo, J.T.: Static response of a multilayered medium under inclined surface loads. J. Geophys. Res. **74**, 3195–3207, 1969

Lambeck, K., Nakiboglu, S.M.: Seamount loading and stress in the ocean lithosphere. J. Geophys. Res. **85**, 6403–6418, 1980

Lanczano, P.: Deformations of an elastic Earth. New York: Academic Press 1982

McConnell, R.K. jr.: Isostatic adjustment in a layered Earth. J. Geophys. Res. **70**, 5171–5188, 1965

McConnell, R.K. jr.: Viscosity of the mantle from relaxation time spectra of isostatic adjustment. J. Geophys. Res. **73**, 7089–7105, 1968

Nakiboglu, S.M., Lambeck, K.: A study of the Earth's re-

sponse to surface loading with application to Lake Bonneville. Geophys. J.R. Astron. Soc. **70**, 577–620, 1982
Parker, R.L.: The rapid calculation of potential anomalies. Geophys. J.R. Astron. Soc. **31**, 447–455, 1972
Parsons, B.E.: Changes in the Earth's shape. Ph.D. thesis, Cambridge University 1972
Peltier, W.R.: The impulse response of a Maxwell Earth. Rev. Geophys. Space Phys. **12**, 649–669, 1974
Peltier, W.R.: Glacial-isostatic adjustment – II. The inverse problem. Geophys. J.R. Astron. Soc. **46**, 669–705, 1976
Peltier, W.R.: Dynamics of the ice age Earth Adv. Geophys. **24**, 1–146, 1982
Peltier, W.R.: The LAGEOS constraint on deep mantle viscosity: results from a new normal mode method for the inversion of viscoelastic relaxation spectra. J. Geophys. Res. 1985 (in press)
Peltier, W.R., Andrews, J.T.: Glacial-isostatic adjustment – I. The forward problem. Geophys. J.R. Astron. Soc. **46**, 605–646, 1976
Sclater, J.G., Jaupart, C., Galson, D.: The heat flow through oceanic and continental crust and the heat loss of the Earth. Rev. Geophys. Space Phys. **18**, 269–311, 1980
Tullis, J.A.: High temperature deformation of rocks and minerals. Rev. Geophys. Space Phys. **17**, 1137–1154, 1979
Walcott, R.I.: Rheological models and observational data of glacio-isostatic rebound. In: Earth rheology, isostasy, and eustasy, N.-A. Mörner, ed.: pp. 3–10. New York: Wiley 1980
Ward, S.N.: A note on lithospheric bending calculations. Geophys. J.R. Astron. Soc. **78**, 241–253, 1984
Weertman, J., Weertman, J.R.: High temperature creep of rock and mantle viscosity. Annu. Rev. Earth Planet. Sci. **3**, 293–315, 1975
Wolf, D.: The relaxation of spherical and flat Maxwell Earth models and effects due to the presence of the lithosphere. J. Geophys. **56**, 24–33, 1984
Wolf, D.: Thick-plate flexure re-examined. Geophys. J.R. Astron. Soc. **80**, 265–273, 1985a
Wolf, D.: On Boussinesq's problem for Maxwell continua subject to an external gravity field. Geophys. J.R. Astron. Soc. **80**, 275–279, 1985b
Wolf, D.: The normal modes of a uniform, compressible Maxwell half-space. J. Geophys. **56**, 100–105, 1985c
Wolf, D.: An improved estimate of lithospheric thickness based on a reinterpretation of tilt data from Pleistocene Lake Algonquin. Can. J. Earth Sci. 22, 768–773, 1985d
Wu, P., Peltier, W.R.: Viscous gravitational relaxation. Geophys. J.R. Astron. Soc. **70**, 435–485, 1982
Wu, P., Peltier, W.R.: Glacial isostatic adjustment and the free-air gravity anomaly as a constraint on deep mantle viscosity. Geophys. J.R. Astron. Soc. **74**, 377–449, 1983

Received February 11, 1985; revised version April 23, 1985
Accepted April 25, 1985